PROCEEDINGS OF SCIENCE

TeV-PeV Cosmic-Ray Anisotropy as a Probe of the Local Interstellar Turbulence

Gwenael Giacinti*
Max-Planck-Institut für Kernphysik, Postfach 103980, 69029 Heidelberg, Germany
E-mail: giacinti@mpi-hd.mpg.de

John G. Kirk
Max-Planck-Institut für Kernphysik, Postfach 103980, 69029 Heidelberg, Germany
E-mail: john.kirk@mpi-hd.mpg.de

We calculate the large-scale cosmic-ray (CR) anisotropies predicted for a range of Goldreich-Sridhar (GS) and isotropic models of interstellar turbulence, and compare them with IceTop data. In general, the predicted CR anisotropy is not a pure dipole; the cold spots reported at 400 TeV and 2 PeV are consistent with a GS model that contains a smooth deficit of parallel-propagating waves and a broad resonance function, though some other possibilities cannot, as yet, be ruled out. In particular, isotropic fast magnetosonic wave turbulence can match the observations at high energy, but cannot accommodate an energy dependence in the shape of the CR anisotropy. Our findings suggest that measurements of the large-scale CR anisotropy may be used as a local probe of the properties of the interstellar turbulence (notably its power-spectrum), and of CR transport, within a few tens of parsecs from Earth.

35th International Cosmic Ray Conference — ICRC2017
10–20 July, 2017
Bexco, Busan, Korea

*Speaker.

PoS(ICRC2017)578

1. Introduction

In this paper we report on investigations of how the *shape* of the large-scale (LS) anisotropy of TeV–PeV cosmic-rays, (i.e., excluding features whose angular sizes are smaller than a few tens of degrees) depends on the properties of the interstellar turbulence and cosmic ray (CR) transport within $\sim 10\,\mathrm{pc}$ from Earth [1]. Up until now, most studies of the large-scale CR anisotropy (CRA) have focussed on the *direction* and *amplitude* of the *dipole*, and in particular its relation to local sources of CRs (for a recent study see e.g. [2]). The direction of the CRA is observed to be compatible with that of the local interstellar magnetic field, as deduced from the IBEX ribbon and from polarization of starlight from stars within ten to a few tens of pc from Earth [3, 4, 5]. However, the LS CRA is not well described by a dipole [6]. A few earlier studies have modeled phenomenologically the LS CRA as the sum of a dipole and higher order multipoles (e.g. [7]), but the study we present here is, to our knowledge, the first quantitative description linking it to the power-spectrum and other parameters of the turbulence.

2. Large-scale cosmic-ray anisotropy

The alignment of the CRA with local field lines within $\sim 10\,\mathrm{pc}$ [3] is compatible with the widely held view that CRs diffuse preferentially along field lines. Ref. [3] suggests that the power in the fluctuations on which TeV–PeV CRs scatter ($\sim 10^{-4} - 1\,\mathrm{pc} \ll 10\,\mathrm{pc}$) is small with respect to that in this ordered field. We therefore assume pitch-angle diffusion of CRs in a $\sim 10\,\mathrm{pc}$-long, uniform flux tube containing the Earth. Assuming the turbulence to be homogeneous, and the problem to be 1D and stationary, the pitch-angle distribution of CRs $f(z,\mu)$ satisfies

$$\mu v \frac{\partial f}{\partial z} = \frac{\partial}{\partial \mu}\left(D_{\mu\mu} \frac{\partial f}{\partial \mu} \right) , \tag{2.1}$$

where z is the spatial coordinate along the tube, μ is the cosine of the CR pitch-angle (angle between the CR momentum and the ordered magnetic field), $D_{\mu\mu}$ the pitch-angle diffusion coefficient, and $v = c$. We place the Earth at $z = 0$, set the tube boundaries at $z = \pm d \sim \pm 10\,\mathrm{pc}$, and impose a non-zero CR flux along z. Around $z = 0$ —cf. [8],

$$f(z,\mu) = a_{\mathrm{diff}}\left[z + \tilde{g}(\mu) \right] , \tag{2.2}$$

provided that the boundaries are sufficiently far, i.e.

$$\exp\left(-\Lambda_1 d / v \right) \ll 1 , \tag{2.3}$$

where Λ_1 is the smallest, non-zero, positive eigenvalue of (2.1), a_{diff} a constant, and $\tilde{g}$ a solution of $\partial\left(D_{\mu\mu} \partial \tilde{g} / \partial \mu \right) / \partial \mu = v\mu$. See [1] for a delimitation of the parameter space where Eq. (2.3) is satisfied. Outside this range, f is determined by the unknown boundary conditions —see [9] for an application to small scale anisotropies. In the following, we assume that (2.3) is satisfied. Then, *the CRA at Earth is proportional to* $\tilde{g}(\mu)$. Imposing $\int_{-1}^{1} \mathrm{d}\mu\, \tilde{g} = 0$,

$$\tilde{g}(\mu) = -\frac{v}{2} \int_0^{\mu} \mathrm{d}\mu' \, \frac{1 - \mu'^2}{D_{\mu'\mu'}} , \tag{2.4}$$

cf. [1]. Since we study here the shape of the CRA, and not its absolute amplitude, we work with the anisotropy normalized to 1,

$$g(\mu) = \frac{\tilde{g}(\mu)}{\tilde{g}(1)}. \tag{2.5}$$

$D_{\mu\mu}$ can be expressed in terms of a (phenomenological) resonance function, R_n —see e.g. [10, 11]:

$$D_{\mu\mu} = \Omega^2 \left(1-\mu^2\right) \int \mathrm{d}^3 k \sum_{n=-\infty}^{\infty} \left(\frac{n^2 \mathrm{J}_n^2(y)}{y^2} I_{\mathrm{A}}(\mathbf{k}) + \frac{k_\parallel^2 \mathrm{J}_n'^2(y)}{k^2} I_{\mathrm{S,F}}(\mathbf{k}) \right) \times R_n \,, \tag{2.6}$$

where $I_{\mathrm{A,S,F}}$ are the normalized energy spectra of the Alfvén (A), slow or pseudo-Alfvén (S), and fast (F) modes. Ω is the CR gyrofrequency, $y = k_\perp l \varepsilon \sqrt{1-\mu^2}$, $k_\perp$ is the component of the wavevector $\mathbf{k}$ perpendicular to the magnetic field, l the outer scale of the turbulence, and $\varepsilon = v/l\Omega = r_{\mathrm{L}}/l$ the dimensionless CR rigidity. The physically unfounded case of isotropic pitch-angle scattering would correspond to a constant pitch-angle scattering frequency $\nu(\mu) = 2D_{\mu\mu}/(1-\mu^2) \times (l/v) = \mathrm{cst}$, and to a pure dipole anisotropy, $g(\mu) = \mu$.

We use broad (R_n^{B}) and narrow (R_n^{N}) resonance functions, taken respectively from [12] and [13]:

$$R_n^{\mathrm{B}} = \frac{\sqrt{\pi}}{\left|k_\parallel\right| v_\perp \delta M_{\mathrm{A}}^{1/2}} \exp\left(-\frac{(k_\parallel v_\parallel - \omega + n\Omega)^2}{k_\parallel^2 v_\perp^2 \delta M_{\mathrm{A}}} \right)$$

$$R_n^{\mathrm{N}} = \frac{\tau^{-1}}{(k_\parallel v_\parallel - \omega + n\Omega)^2 + \tau^{-2}} \,, \tag{2.7}$$

where $v_\parallel = v\mu$, $v_\perp = v\sqrt{1-\mu^2}$, ω is the angular frequency of the waves, and $k_\parallel$ the parallel component of $\mathbf{k}$. R_n^{B} takes into account the broadening of the resonance due to fluctuations of the magnetic field strength. This is encapsulated in the parameter $\delta M_{\mathrm{A}} \lesssim 1$, whose local value is poorly constrained. R_n^{N} assumes instead that the broadening of the resonance, described by τ, is dominated by the Lagrangian correlation time of the turbulence.

3. Results

We use here models with $D_{\mu\mu}(-\mu) = D_{\mu\mu}(\mu)$. Thus, $\nu(-\mu) = \nu(\mu)$ and $g(-\mu) = -g(\mu)$, and we plot ν and g on $0 \leq \mu \leq 1$ only. Typically, $l \sim (1-100)\,\mathrm{pc}$, so the dimensionless CR rigidity $\varepsilon = v/l\Omega$ is $\sim 10^{-4} - 10^{-1}$ for $\sim$ PeV CRs. We assume that the field points in the direction $(l,b) = (47^\circ, 25^\circ)$, which is compatible with [4].

3.1 Goldreich-Sridhar turbulence

First, we consider Goldreich-Sridhar (GS) turbulence [14], with a spectrum of Alfvén and pseudo-Alfvén waves following the prescription of [15]: $I_{\mathrm{A,S}}(\mathbf{k}) \propto k_\perp^{-10/3} \exp(-k_\parallel l^{1/3}/k_\perp^{2/3})$. In Ref. [1], we also studied spectra with an abrupt cutoff in $k_\parallel$ and found qualitatively similar trends. The resonance function R_n^{N} provides so little scattering that the CRA is given by $g(\mu)$ only in a small fraction of parameter space, in which it anyway does not fit IceTop data. For GS turbulence, we then only use R_n^{B}. We calculate numerically $D_{\mu\mu}$, and plot $\nu(\mu)$ (resp. the CRA, $g(\mu)$) in the upper left (resp. centre) panel of Fig. 1, for 3 sets of values of $\{\varepsilon, \delta M_{\mathrm{A}}\}$ that fit well IceTop

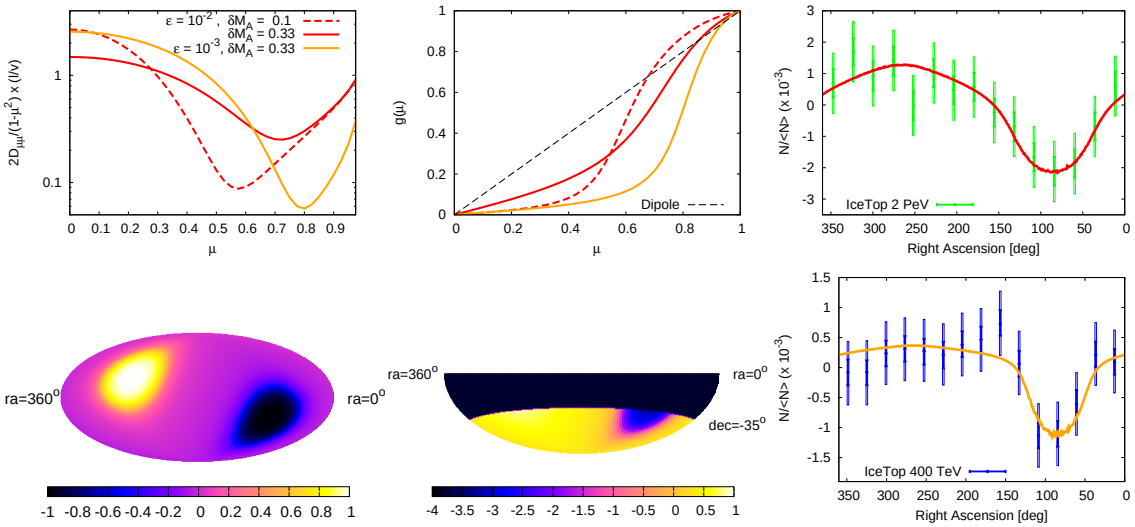

Figure 1: GS turbulence with $R_n^{\rm B}$: $\nu(\mu)$ (*upper left panel*), $g(\mu)$ (*upper centre*), and relative CR intensity at $-75^\circ \leq$ decl. $\leq -35^\circ$ versus R.A., compared with the 2 PeV (resp. 400 TeV) data from IceTop (*upper right, resp. lower right*). See upper left panel for the parameters of each set of lines. *Lower left panel:* Anisotropy g in equatorial coordinates for $\varepsilon = 10^{-3}$ and $\delta M_{\rm A} = 0.33$. *Lower centre panel:* CRA in the field of view of IceTop (calculated with respect to the average flux in each declination band) for the same ε and $\delta M_{\rm A}$, and with minimum amplitude renormalized to -1.

data [6]: $\{10^{-2}, 0.1\}$ (red dashed line), $\{10^{-2}, 0.33\}$ (red solid), $\{10^{-3}, 0.33\}$ (orange solid). For these parameters, ν exhibits a minimum in the range $|\mu| \simeq 0.55 - 0.8$ which corresponds to the transition between two regions: At smaller $|\mu|$ (i.e. perpendicular to field lines), scattering is dominated by the $n = 0$ contribution of pseudo-Alfvén modes, whereas at larger $|\mu|$, Alfvén modes dominate. At fixed ε, and when $\delta M_{\rm A}$ increases, the minimum of ν occurs at larger $|\mu|$, cf. the two red lines. Indeed, the width of the bump around $\mu = 0$ increases for broader resonances. The minimum of ν corresponds to the sharp increase of g at large μ, see centre panel and Eq. (2.4). This leads to excesses/deficits in the CRA along field lines ($\mu = \pm 1$) that are narrower than for a dipole (black dashed line). We plot the anisotropy in (R.A., decl.) for $\{10^{-3}, 0.33\}$ in the lower left panel. Tight cold/hot spots are present along the field, and a rather wide flat region lies in-between (magenta). This leads to a Southern sky map similar to what IceTop observes (lower centre panel): A narrow cold spot (dark blue) surrounded with a flat CR intensity. The two right panels show our predicted relative intensities at $-75^\circ \leq$ decl. $\leq -35^\circ$ versus IceTop data sets for a *fixed* set of turbulence parameters ($\delta M_{\rm A} = 0.33$): At low CR energy ($\varepsilon = 10^{-3}$), we can fit well the 400 TeV data, and by increasing the energy by a factor 10 ($\varepsilon = 10^{-2}$) —comparable to the factor 5 in the data, the 2 PeV data is also well fitted. We note that the existing data can also exclude a non-negligible range of possible parameter values, see [1] for a wider scan.

3.2 Isotropic Fast modes

Second, we study isotropic fast mode turbulence with a power spectrum $I_{\rm F}(k) \propto k^{-3/2}$, as suggested by [16]. In Fig. 2, we plot ν (left), g (centre), and the relative CR intensity at $-75^\circ \leq$ decl. $\leq -35^\circ$ versus IceTop 2 PeV data (right). We consider $R_n^{\rm B}$ with $\delta M_{\rm A} = 0.01$ (blue dashed-

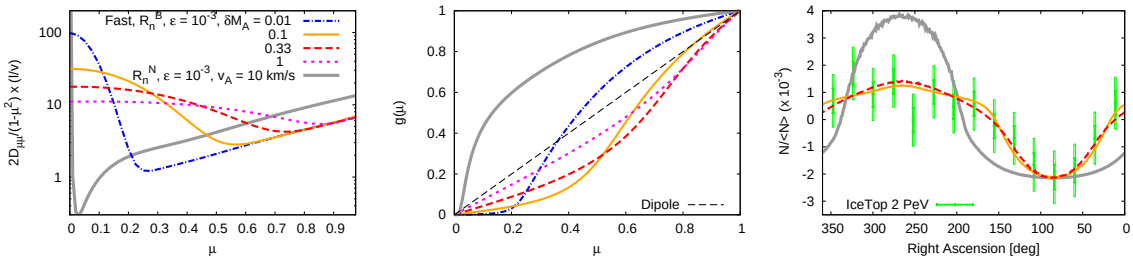

Figure 2: Isotropic fast modes: $\nu(\mu)$ (*left panel*), $g(\mu)$ (*center panel*), and relative CR intensity at $-75^\circ \leq$ decl. $\leq -35^\circ$ versus R.A., compared with the 2 PeV data from IceTop (*right panel*). See left panel for the parameters of each set of lines.

dotted lines), 0.1 (orange solid), 0.33 (red dashed), 1 (magenta dotted), as well as $R_n^{\rm N}$ for a local Alfvén velocity $v_{\rm A} = 10$ km/s (grey solid), and with $\tau = \sqrt{l}/v_{\rm A}\sqrt{k}$. We take $\varepsilon = 10^{-3}$ for the plot of $\nu(\mu)$. We find that g does not depend on ε here. As for pseudo-Alfvén modes above, the $n = 0$ term for fast modes is now responsible for the peak of ν around $\mu = 0$. This peak grows in width when $\delta M_{\rm A}$ increases. With the narrow resonance function, it becomes very sharp and the minimum of ν is close to $\mu = 0$, see grey line. This results in a qualitatively different shape of the CRA, cf. middle panel: Very wide cold/hot spots with a rather flat intensity inside. They take nearly half of the sky each ($\simeq 80^\circ$ half-width). IceTop data clearly rules out this *a priori* acceptable scenario, cf. right panel. For $R_n^{\rm B}$, the 2 PeV data is well fitted with $\delta M_{\rm A} = 0.1$ and 0.33, where the deficit at R.A. $\approx 90^\circ$ reaches its minimum width. However, the 400 TeV data is not well fitted. Decreasing $\delta M_{\rm A}$ makes the deficit too wide (blue lines), while increasing $\delta M_{\rm A}$ to 1 (magenta lines) makes the anisotropy tend towards a dipole, which again increases the size of the deficit.

4. Discussion

In all models above, the CRA exhibits a flattening in directions perpendicular to field lines, due to the peak of the scattering frequency around $\mu = 0$. Interestingly, this signature is compatible with the observational data. Moderately broad resonance functions are able to produce deficits/excesses along the field direction ($\mu = \pm 1$) that are narrower than those of a dipole. Too broad a resonance would, however, result in an approximately dipole anisotropy with constant ν, see the magenta lines in Fig. 2. On the other hand, narrow resonance functions are disfavoured by IceTop data. Nonetheless, we cannot formally exclude narrow resonance functions for models of turbulence in which ν is so small that the CR mean free path is $\gg 100$ pc, such as in [13], since our study does not then apply. A very low CR scattering rate locally is not impossible, but shifts the problem of CR confinement and the explanation of its anisotropy to large distance. The increase with CR energy of the width of the deficit between the two IceTop data sets may hint at a $|\mathbf{k}|$-dependent anisotropy in the turbulence power-spectrum, such as in GS turbulence. Other possibilities, such as an energy-dependence of the resonance function should also be explored. As for fast modes, they should suffer from damping [12], which we did not take into account, and which may have an effect on the CRA. A combined analysis of all available CRA data (notably [17]) should yield tighter constraints than those presented in Sect. 3. Distortions of the CRA by heliospheric fields [18, 19] may complicate the picture at $\lesssim 10$ TeV. The recent data from the Tibet Air Shower Array [20]

hints at the presence of a narrow hot spot in the Northern hemisphere, in their 300 TeV data set (cf. their Fig. 4), as would be expected within our model and for a $D_{\mu\mu}$ symmetric with respect to $\mu = 0$.

5. Conclusions

Assuming pitch-angle diffusion of Galactic CRs in our local environment, we deduced the shape of the LS CRA, see Eqs. (2.4) and (2.5). In general, it is not a pure dipole, but contains imprints of the still poorly known properties of (i) the local interstellar turbulent magnetic fields (e.g. power-spectrum), and (ii) CR transport (via R_n). We find that the existing observational data already puts constraints on these. A *moderately* broad resonance function seems to be favoured. IceTop 2 PeV data can be fitted either with GS turbulence or isotropic fast modes (see parameters in Figs. 1 and 2), but only the former can reproduce the change in the width of the deficit between the 400 TeV and 2 PeV data sets. We suggest that the shape of the large-scale cosmic-ray anisotropy can be used as a new observable.

References

[1] G. Giacinti, J. G. Kirk, *Large-Scale Cosmic-Ray Anisotropy as a Probe of Interstellar Turbulence*, *ApJ* **835** (2017) 258 [arXiv:1610.06134].

[2] M. Ahlers, *Deciphering the Dipole Anisotropy of Galactic Cosmic Rays*, *Physical Review Letters* **117** (2016) 151103 [arXiv:1605.06446].

[3] N. A. Schwadron, F. C. Adams, E. R. Christian, P. Desiati, P. Frisch, H. O. Funsten, J. R. Jokipii, D. J. McComas, E. Moebius, G. P. Zank, *Global Anisotropies in TeV Cosmic Rays Related to the Sun's Local Galactic Environment from IBEX*, *Science* **343** (2014) 988–990.

[4] P. C. Frisch, B.-G. Andersson, A. Berdyugin, V. Piirola, R. DeMajistre, H. O. Funsten, A. M. Magalhaes, D. B. Seriacopi, D. J. McComas, N. A. Schwadron, J. D. Slavin, S. J. Wiktorowicz, *The Interstellar Magnetic Field Close to the Sun. II.*, *ApJ* **760** (2012) 106 [arXiv:1206.1273].

[5] P. C. Frisch, A. Berdyugin, V. Piirola, A. M. Magalhaes, D. B. Seriacopi, S. J. Wiktorowicz, B.-G. Andersson, H. O. Funsten, D. J. McComas, N. A. Schwadron, J. D. Slavin, A. J. Hanson, C.-W. Fu, *Charting the Interstellar Magnetic Field causing the Interstellar Boundary Explorer (IBEX) Ribbon of Energetic Neutral Atoms*, *ApJ* **814** (2015) 112 [arXiv:1510.04679].

[6] M. G. Aartsen, R. Abbasi, Y. Abdou, M. Ackermann, J. Adams, J. A. Aguilar, M. Ahlers, D. Altmann, K. Andeen, J. Auffenberg, et al., *Observation of Cosmic-Ray Anisotropy with the IceTop Air Shower Array*, *ApJ* **765** (2013) 55 [arXiv:1210.5278].

[7] M. Zhang, P. Zuo, N. Pogorelov, *Heliospheric Influence on the Anisotropy of TeV Cosmic Rays*, *ApJ* **790** (2014) 5.

[8] N. J. Fisch, M. D. Kruskal, *Separating variables in two-way diffusion equations*, *J. Math. Phys.* **21** (1980) 740.

[9] M. A. Malkov, P. H. Diamond, L. Drury, R. Z. Sagdeev, *Probing Nearby Cosmic-ray Accelerators and Interstellar Medium Turbulence with MILAGRO Hot Spots*, *ApJ* **721** (2010) 750.

[10] R. Kulsrud, W. P. Pearce, *The Effect of Wave-Particle Interactions on the Propagation of Cosmic Rays*, *ApJ* **156** (1969) 445.

[11] H. J. Völk, *Nonlinear Perturbation Theory for Cosmic Ray Propagation in Random Magnetic Fields*, *Ap&SS* **25** (1973) 471.

[12] H. Yan, A. Lazarian, *Cosmic-Ray Propagation: Nonlinear Diffusion Parallel and Perpendicular to Mean Magnetic Field*, *ApJ* **673** (2008) 942–953 [arXiv:0710.2617].

[13] B. D. G. Chandran, *Scattering of Energetic Particles by Anisotropic Magnetohydrodynamic Turbulence with a Goldreich-Sridhar Power Spectrum*, *Physical Review Letters* **85** (2000) 4656–4659 [arXiv:astro-ph/0008498].

[14] P. Goldreich, S. Sridhar, *Toward a theory of interstellar turbulence. 2: Strong alfvenic turbulence*, *ApJ* **438** (1995) 763–775.

[15] J. Cho, A. Lazarian, E. T. Vishniac, *Simulations of Magnetohydrodynamic Turbulence in a Strongly Magnetized Medium*, *ApJ* **564** (2002) 291–301 [arXiv:astro-ph/0105235].

[16] J. Cho, A. Lazarian, *Compressible Sub-Alfvénic MHD Turbulence in Low-β Plasmas*, *Physical Review Letters* **88** (2002) 245001 [arXiv:astro-ph/0205282].

[17] M. G. Aartsen *et al.* [IceCube Collaboration], *Anisotropy in Cosmic-ray Arrival Directions in the Southern Hemisphere Based on six Years of Data From the Icecube Detector*, *ApJ* **826** (2016) 220 [arXiv:1603.01227].

[18] P. Desiati and A. Lazarian, *Anisotropy of TeV Cosmic Rays and the Outer Heliospheric Boundaries*, *ApJ* **762** (2013) 44 [arXiv:1111.3075].

[19] L. Drury, *The problem of small angular scale structure in the cosmic ray anisotropy data*, In Proceedings of the 33rd International Cosmic Ray Conference (Rio de Janeiro, Brazil, 2013) [arXiv:1305.6752].

[20] M. Amenomori, X. J. Bi, D. Chen, T. L. Chen, W. Y. Chen, S. W. Cui, Danzengluobu, L. K. Ding, C. F. Feng, Z. Feng et al., The Tibet ASγ Collaboration, *Northern Sky Galactic Cosmic Ray Anisotropy between 10 and 1000 TeV with the Tibet Air Shower Array*, *ApJ* **836** (2017) 153 [arXiv:1701.07144].